Experimental tests and radiometric calculations for the feasibility of fluorescence LIDAR detection of oil spills from UAV

Valentina Raimondi[1*], Lorenzo Palombi[1], David Lognoli[1], Andrea Masini[2] and Emilio Simeone[2]

[1] "Nello Carrara" Applied Physics Institute of the National Research Council of Italy (CNR-IFAC), Sesto Fiorentino (Italy)

[2] FLYBY srl, Livorno (Italy)

Corresponding author:

Valentina Raimondi

'Nello Carrara' Institute of Applied Physics - National Research Council of Italy (CNR-IFAC)

Via Madonna del Piano, 10

I-50019 Sesto Fiorentino (Firenze)

Italy

e-mail: v.raimondi@ifac.cnr.it

phone: +39-055-5226379

fax: +39-055-5226328

ABSTRACT

This paper presents experimental tests and radiometric calculations for the feasibility of an ultra-compact fluorescence LIDAR to be deployed from an Unmanned Air Vehicle (UAV) for the detection and characterisation of oil spills in natural waters. The first step

of this study was to define the experimental conditions for the operation of the LIDAR from UAV and the relevant budget constraints. The latter were retrieved from the main technical characteristics of a selection of small UAVs already available on the market for commercial use. The second step consisted in a set of fluorescence measurements on oil spills in the laboratory by using a fluorescence LIDAR to propose a simplified discrimination method, taking also into account a review of the fluorescence-based methods and a preliminary survey of the technologies available on the market. The laboratory measurements were also used to calculate the oil fluorescence conversion efficiency. Finally, the payload main technical specifications were defined and radiometric calculations carried out to evaluate the performances of the payload and of the proposed discrimination method.

KEYWORDS: fluorescence LIDAR; remote sensing; oil spills; marine pollution; fluorescence spectra; UAV

HIGHLIGHTS

- Oil fluorescence conversion efficiencies were measured for different types of oil samples.
- A simplified fluorescence-based method for oil discrimination, based on ratios between a limited number of spectral bands, was identified.
- Radiometric calculations for UAV-based fluorescence LIDAR were carried out and the proposed method was evaluated at an operational altitude of 200 m.

1. INTRODUCTION

Fluorescence LIDAR is widely regarded as a useful technique for the early detection and classification of oil spills thanks to their characteristic fluorescence spectral shape and lifetime (Fantasia and Ingrao, 1974; Measures et al, 1974; Brown and Fingas, 2003; Hegazi et al, 2005; Palombi et al. 2013).

Fluorescence spectroscopic methods for the detection and classification of oil spills are essentially based on measurements of the fluorescence intensity, fluorescence lifetime or the analysis of the fluorescence spectral distribution. The classification methods based on the analysis of fluorescence spectral distribution require the acquisition of fluorescence data with an adequate spectral resolution. These methods rely on the evaluation of the position (wavelength) of the fluorescence maximum. The latter can be correlated with the density of the crude oil (Hagemann *et al.* 1986) or its aromatic and saturated concentration (Stasiuk *et al.* 1997). Fluorescence spectral width can also be correlated with the API gravity parameter of the oil. A study addressing a selection of oils from the North Sea has demonstrated a correlation between the emission band width and the API grade using a LED at 380-nm as an excitation source (Ryder, 2002). Another parameter that can be used for oil classification is the ratio between the 650-nm centred red band and the 500-nm centred green band of the fluorescence emission spectrum (Alpem et al 1993). This parameter shows a good correlation with oil viscosity and is linearly dependent on oil density. This parameter has been used also to discriminate different oils and to analyse hydrocarbons containing fluid inclusions; however, it depends on the wavelength used for the excitation of the fluorescence and thus its performance cannot be directly compared with the results obtained with other methods using a different excitation wavelength. An effective method based on spectral band ratios is the QFT-II method developed by the Texaco (Delaune et al., 1999). This method relies on an excitation wavelength of 254 nm to measure the fluorescence

intensities at 287 nm and 365 nm. This method – specifically developed for in-field application - has been applied to a set of 70 types of crude oils demonstrating the feasibility of evaluation of the API grade of the oil, but it is suitable for heavy crude oils (API grade < 15). An additional method based on spectral band ratios uses the ratio between the 535 nm - 750 nm emission band and the 430-535 nm emission band obtained using a 365 nm excitation. This method has been used to classify crude oils, but its accuracy has not been evaluated yet (Pradier et al 1990; Guilhaumou et al 1990). Other studies have addressed the use of synchronous scanning fluorescence spectroscopy for oil fingerprinting (Pharr et al 1993).

If the classification of the oil is not a main goal, oil discrimination or its identification within a predetermined database can be also achieved by applying multivariate statistics techniques such as Principal Component Analysis (PCA). Actually, fluorescence emission, due to the aromatic hydrocarbons, is strongly affected by the chemical composition (fluorophores and quenchers) and by the physical characteristics (viscosity and optical density) of the oil. As a consequence, the complexity and mixing of several different phenomena, such as absorption, energy transfer and reabsorption, produces a wide variety of spectral distributions that are typical of the oil itself. This method is also useful to detect the small modifications in the spectral shape of the fluorescence that are caused by the weathering of the oil spill and thus can be exploited to monitor its temporal evolution along time. Spectral matching algorithms based on similarity and dissimilarity criteria have been applied to a dataset of 9 different crude oils and diesel and demonstrated to discriminate amongst 5 samples. The discrimination of the other four samples has been obtained by applying the PCA. The latter has also allowed for the monitoring of the temporal evolution of the oil spill weathering (Li et al 2004).

Another very interesting method of classification is based instead on the measurement of the fluorescence lifetime of the oil components that have fluorescence lifetimes ranging between 1 ns and 20 ns (Camagni et al 1988; Hegazi et al 2005). This type of technique, which is also suitable for remote sensing applications, is based on the measurement of the average lifetime of fluorescence of the oils at different emission wavelengths. Generally, the technique is applied using a pulsed laser as an excitation source in the UV (typically, a frequency-tripled Nd: YAG laser). The use of this method, however, requires complex instrumentation since the latter must feature both spectral and temporal resolution (Camagni et al, 1988; Hegazi et al, 2005).

Besides oil classification or discrimination, the fluorescence LIDAR technique offers other advantages with respect to other techniques (Goodman 1994, Jha et al, 2008). One of these is the possibility to evaluate the thickness of the oil spill, which is important to assess the quantity of the oil spilled into the water. These methods are mainly based on the study of the water Raman signal (Hoge and Swift, 1980; Reuter et al 1995; Chubarov et al 1995; Piskozub et al 1997; Patsayeva et al 2000; Brown and Fingas, 2003). In addition, fluorescence LIDAR technique is also particularly useful for its capability to detect oil spills also in complex scenarios, such as oil under water surface, water-oil emulsions and also unconventional backgrounds such as shorelines, weeds and ice (Patsayeva et al 1997; Balick et al 1997). Up to now, however, the deployment of fluorescence LIDARs for oil spill detection has been limited to conventional airborne platforms, mainly due the payload's budgets in terms of weight, consumption and dimensions (Lennon et al, 2005; Masahiko 2005). In recent years, however, the ever growing availability of compact and efficient laser sources and detectors has opened new perspectives for the design and development of airborne very compact LIDAR systems.

This paper presents experimental tests and radiometric calculations for the feasibility of an ultra-compact fluorescence LIDAR to deploy from an Unmanned Air Vehicle (UAV) for the detection and discrimination of oil spills in natural waters.

The first step undertaken was to outline the experimental conditions for the operation of the LIDAR from UAV and an evaluation of the budget constraints given by the operation from UAV platforms. The latter was achieved by taking into account the main technical characteristics of a selection of small UAVs already available on the market for commercial use.

The second step consisted in a review of fluorescence-based oil detection, classification and discrimination methods available in the literature in order to evaluate the impact of their requirements in terms of instrumentation performances (e.g. spectral resolution, temporal resolution availability, etc.). Subsequently, a set of fluorescence measurements on oil spills in the laboratory by using a fluorescence LIDAR were carried out to propose a simplified discrimination algorithm, taking into account the review of the fluorescence-based methods and a preliminary survey of the technologies available on the market for the development of a ultra-compact LIDAR. The laboratory experiments were also exploited to calculate the oil fluorescence conversion efficiency.

Finally, taking into account the results of the laboratory measurements and the constraints set by available technologies and operational conditions, the payload main technical specifications were defined. On the base of the retrieved oil conversion efficiencies and the payload technical specifications, radiometric calculations were carried out for an assessment of the payload performances and of the proposed discrimination algorithm.

2. OPERATIONAL SCENARIO

The first phase of this study consisted in outlining a consistent operational scenario for the UAV-based LIDAR system: this was done by taking into account typical operational conditions expected in the field and the main technical characteristics of the platform, the latter introducing several constraints on the LIDAR requirements. The definition of operational scenario is required to define the parameters needed for the radiometric calculations and to outline the main technical requirements for the LIDAR system.

The main parameters considered for the definition of these scenarios were: (1) type of seepage into the sea, (2) type of oil or derivates, (3) status of the spill, (4) flight altitude of the platform, and (5) observation geometry.

In this study, a typical scenario constituted by an accidental seepage of crude oil into the sea was considered. The crude oil contains a large variety of light to heavy compounds and thus crude oil spills are subject to several physical and mechanical actions. In the first 24 hours after the spillage the evaporation process can remove about a third of the volume of a crude oil spill. As a consequence, in this case the weathering of the oil spill is particularly meaningful. A similar scenario is the spillage of fuel (such as gasoline, mixture, gas oil) by recreational vessels. The fuels used in the recreational boating are mixtures of gasoline and lubricating oil in variable ratios. The bulk of the fuel, gasoline, is a light fraction and evaporates quickly from the water surface. The lubricating oil mixed with the petrol originates films and layers which tend to evaporate and dissolve.

The selection of the type of oils was consistent with the choice of these scenarios. Several thicknesses of the oil spill were also considered, also because they can affect the weathering of the oil spill and the behaviour of fluorescence spectral distribution along time.

As for the flight altitude of the platform, this was chosen after a preliminary survey carried out to identify a possible UAV platform that could fit the operational conditions outlined for the system. Key constraints given by the platform are the allowances for the payload weight, consumption and dimensions, but also minimum flight altitude and cruising speed.

The main technical characteristics of the UAV platform considered in this study are reported in Table 1. These are compatible with several models of UAV already available on the market for commercial use.

Table 1. The main technical characteristics of the UAV platform.

Parameter	**Value**
Payload weight (maximum)	6 - 13 kg
Cruising speed	< 30 km/h
Minimum altitude	100 m
Maximum altitude	2800 - 3000 m
Endurance	1.5 - 3 h
Take-off weight	55 - 90 kg
Takeoff/Landing	5 - 8 m

As for the geometry of observation, a nadir observation was considered for the radiometric calculations.

3. MATERIAL AND METHODS

3.1 Sample preparation

Four different types of oils were selected for the measurements in the laboratory: a crude oil, an automotive diesel fuel, a marine diesel fuel and an automotive gasoline fuel. These samples were used to make oil slicks of various thicknesses ranging from 70 μm to 210 μm. The oil slicks were made by pipetting the pure oils on the surface of synthetic seawater (34 g/l salinity). The oil slicks were prepared in a set of Pyrex beakers (600-ml volume, 86-mm diameter) filled with seawater (about 460 ml). Synthetic seawater was selected as a substrate in order to take into account possible oil-seawater interaction in the determination of the spectral fluorescence behaviour of the oil samples and its weathering. Fluorescence measurements were carried out immediately after oil slick preparation in order to avoid modifications in the oil slick composition due to the evaporation of the lighter fractions and oil weathering effects. A second set of measurements was instead devoted to the study of oil slick weathering along time, in order to evaluate modifications in the fluorescence spectral properties of the oil samples.

3.2 Instrumentation

Spectrally-resolved fluorescence measurements were obtained using an in-house developed fluorescence LIDAR (Raimondi *et alii*, 2008; Palombi *et alii*, 2013). The system uses a tripled-frequency Nd:YAG laser as an excitation source (Continuum, Minilite II, 8-mJ pulse energy, 5-ns pulse width, 15-Hz maximum pulse repetition rate). The laser beam is conditioned by a beam expander and a focusing optics (3X) to reduce its divergence to the field of view of the LIDAR telescope (1 mrad). The laser beam is steered by a couple of dichroic optics that are used to suppress the residual fundamental and doubled frequency components. The second steering optics is used also to make the

excitation beam collinear with the optical axis of the telescope. The beam is sent to a computer-controlled scanning mirror. The fluorescence signal is collected by the telescope (1000-mm focal length, *f*/4) and filtered by a 395-nm long-pass absorption optical filter (Schott GG395) that has the twofold function of rejecting the laser backscattered radiation at 355 nm and avoiding higher-spectral order contributions. The collected and filtered light is focused on an optical fibre bundle (50 silica fibers, 100-μm core diameter, circular-shaped) having a 1-mm diameter. The other end of the optical fibre bundle is coupled to the entrance slit of the spectrometer (PI Acton, SpectraPro 2300i, 300 mm focal length, *f*/3.9) that is equipped with three different and selectable diffraction gratings (150 gg/mm, 600 gg/mm and 2400 gg/mm). The detector is a PI-Acton PI-Max:512 camera (ICCD, Intensified gated CCD, GEN-III, 512 X 512 pixels, 24-μm pixel size). The spectrometer-detector system has a nominal spectral resolution @ 435.8 nm of 0.51 nm/pixel, 0.12 nm/pixel and 0.02 nm/pixel, depending on the diffraction grating used. In this study, the 150-gg/mm diffraction grating was used for acquiring the fluorescence measurements. The fluorescence spectrum in the 350 nm - 810 nm spectral range was obtained by merging two separate acquisitions, the one in the 350 nm – 610 nm range and the other one in the 550 nm – 810 nm range. In addition, in order to increase the signal to noise ratio, the fluorescence spectrum was averaged over 100 laser shots.

3.3 Experimental set-up

The beaker containing the seawater and the oil slick was placed at about 10 m from the LIDAR system. It was placed on a black plastic foil that had a very low fluorescence efficiency so as to avoid possible fluorescence interferences from the background. At this distance the diameter of the area effectively measured by the LIDAR system is 10

mm. An additional folding mirror, placed immediately above the sample, allowed for nadir-observation geometry.

In addition, the evaluation of the fluorescence energy conversion efficiency of the oils (i.e. the ratio between the fluorescence energy - emitted per wavelength unit and per emission solid angle unit - and the energy of the incident radiation) required a radiometric calibration of the LIDAR for this specific measurement set-up. To this purpose, a white reference standard (Spectralon®) was placed at the same position of the oil slick and was homogeneously illuminated by a calibration halogen lamp. The LIDAR radiometric calibration was obtained by comparing the radiance measurements of the LIDAR - used as a passive spectroradiometer (i.e. with the laser off) – and the radiance measurements performed with a calibrated spectroradiometer camera (Photo Research Inc., SpectraPro PR650 model). Instead, the laser fluence on the target was measured by using a calibrated laser energy meter (Gentec, Solo II model).

3.4 Discrimination method

The methods which are best suited for the specific application considered in this study are those based on the analysis of the spectral distribution of the fluorescence and / or on the extent of the fluorescence lifetime. Methods based on the measurement of fluorescence lifetimes, however, were discarded as not compatible with the limited budgets - in terms of weight and dimensions - given by UAV operation. In this respect, the measurement of the spectral distribution is perhaps the method that can be applied more easily from a UAV platform. From this point of view, a method based on the ratios between selected fluorescence spectral bands may offer the additional advantage of significantly reducing the overall dimensions and weight of the dispersion and detection system by means of demultiplexing techniques. As a consequence, the algorithm proposed for oil discrimination was based on the ratios between properly

selected spectral bands. In addition, the number of spectral channels requires for the discrimination was limited as much as possible in order to make easier to fulfil the instrumentation requirements. **Table 2** shows the spectral bands proposed for the oil discrimination.

Table 2. The set of spectral bands selected for oil discrimination.

Name	Spectral range	Measured signal
A	350 - 360 nm	Laser backscattering
B	400 - 410 nm	Water Raman
C	410 – 430 nm	Fluorescence
D	430 – 465 nm	Fluorescence
E	465 – 535 nm	Fluorescence
F	535 – 600 nm	Fluorescence
G	600 – 750 nm	Fluorescence

The selection of the spectral bands took into account also the preliminary technical specifications of the LIDAR system. Specifically, it assumes that the excitation source is a pulsed laser in the UV, since the wavelength of the excitation source determines the choice of the spectral bands of interest, especially as for the channels for the detection of elastic backscattering and the water Raman scattering. Specifically, the spectral bands indicated in Table 2 consider a tripled-frequency Nd: YAG laser @ 355 nm as the excitation source of the LIDAR system.

This set of spectral bands allows the application of several methods amongst those described in the previous section. The ratio between the intensity of the signal

integrated in time between the bands #G and #E has a good correlation with the viscosity of the oil, which is still linearly dependent on its density. This relationship also allows the discrimination between different oils and for the analysis of hydrocarbons containing inclusions of fluids. It is also correlated with a quality parameter of the oil based on the combined concentrations of aromatic fractions, resins and asphaltenes. The ratio between the intensity of the signal integrated in time between the bands #F + #G and #D allows a characterisation of crude oils. In addition, the intensity of the signal integrated over time in the band #B, observed in the presence and in the absence of slick, allows for the estimation of the spill thickness.

The distribution of the intensity of the signal integrated over time in the bands# C, #D, #E, #F and #G can be exploited to reconstruct an approximate spectral distribution of the fluorescence so as to determine the wavelength of maximum emission and its width for an estimate of the degree API and concentrations of saturated and aromatic compounds.

Finally, the number of available bandwidths can potentially enable successful application of methods based on the techniques of multivariate statistics, which can be very useful for a classification of oils, their discrimination and the monitoring of the weathering of the oil spill.

4. RESULTS AND DISCUSSION

A set of measurements was carried out on different oil samples in the laboratory with a twofold aim: (1) to investigate the possibility to discriminate them using a limited number of spectral bands, and (2) to measure their fluorescence conversion efficiencies to carry out the radiometric calculations for an evaluation of the performances of the LIDAR system outlined in this study. Fluorescence spectral behaviour of the oil slick

samples were also studied as a function of slick thickness and of its weathering in order to understand their possible effects on conversion efficiency and discrimination algorithms.

4.1 Oil fluorescence efficiency measurements

Fig. 1 shows the fluorescence energy conversion efficiency of the four oil samples as a function of the wavelength in the 370 nm - 810 nm spectral range. The measured fluorescence energy conversion efficiency - per wavelength unit and per emission solid angle unit – refers to a 100-μm thick slick. The conversion efficiency of the synthetic seawater without oil slick, measured in the same experimental conditions, is also reported for comparison. This includes the water Raman signal due to the OH-stretching of the water molecule, which is placed at about 404 nm for a 355-nm excitation wavelength. The fluorescence efficiency of the four oil samples was measured on an oil slick thickness of 100 μm since this was considered as the minimum thickness needed to obtain a homogenous slick as well as a negligible fluorescence and Raman contribution of the seawater. Actually, in this case the fluorescence intensity of the oil is from 10 times to 50 times more intense than the Raman signal of the seawater.

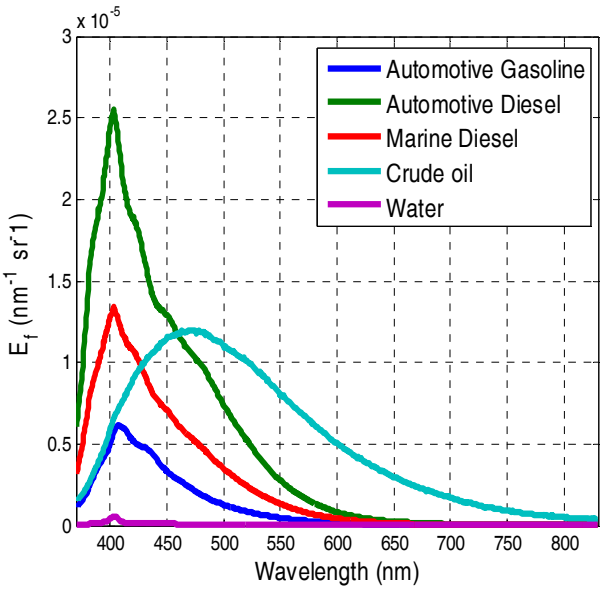

Fig. 1. Fluorescence energy conversion efficiency, as a function of the wavelength, for the four oil samples. The oil slicks were 100-µm thick. The conversion efficiency of the synthetic seawater, including water Raman signal, is also reported.

4.2 Oil samples discrimination

The conversion efficiency is quite different for the four oil samples, both in intensity and – to a lesser extent - in spectral shape. To make easier the comparison of the spectral shapes of the fluorescence efficiency of the four samples, these were normalised to their maximum in Fig. 2.

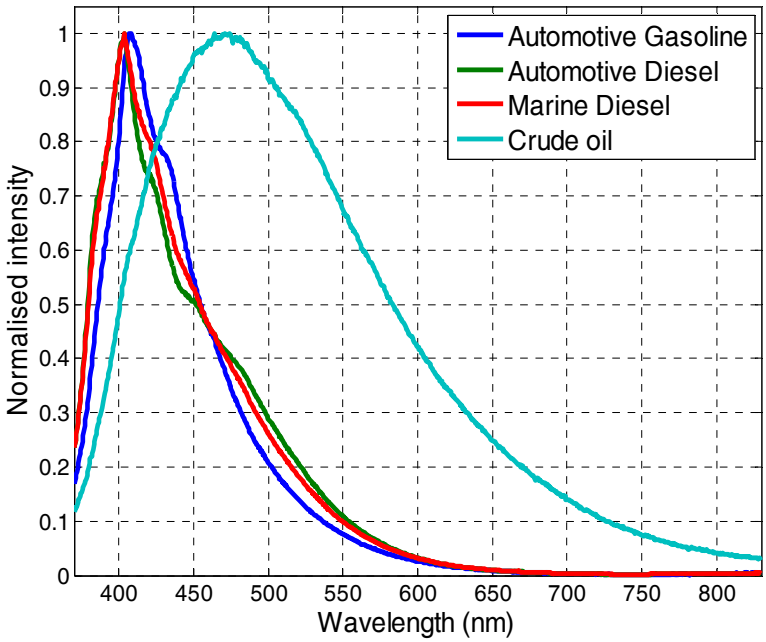

Fig. 2. Fluorescence energy conversion efficiency of the four oil samples normalised to the maximum.

The crude oil, as expected, showed a very different spectral behaviour from the other three samples: it had a maximum at longer wavelengths (about 470 nm) and a larger FWHM (about 200 nm). As a consequence, maximum fluorescence wavelength and fluorescence spectral width can be regarded as parameters suitable for discriminating crude oils from lighter hydrocarbon mixtures, such as fuels. These parameters, however, are not suitable to discriminate the other three samples from each other. The spectral distribution of the diesel samples and of the gasoline fuel sample are quite similar since both show a maximum at about 400 nm and a FWHM of about 75 nm. They, however, show different relative fluorescence contributions at 380 nm, 420 nm, 450 nm and 480 nm. The latter feature can be used for their discrimination by applying spectral band intensity ratios. **Table 3** shows, for each of the four oil samples, the ratio between the

fluorescence intensities integrated in two different spectral ranges chosen amongst those listed in Table 2 and consistently named #C, #D, #E, #F and #G. **Table 3** reports all the possible combinations of ratios (except for the inverse ratios) between the proposed spectral ranges.

Table 3. Ratio between the fluorescence intensities integrated in two different spectral ranges amongst those listed in Table 1. The most suitable ratios for sample discrimination are highlighted.

#	Ratio	Automotive gasoline	Automotive diesel	Marine diesel	Crude oil
1	#D / #C	0.68	0.70	0.68	1.26
2	#E / #C	0.26	0.40	0.34	1.24
3	#F / #C	0.01	0.02	0.02	0.38
4	#G / #C	0.01	0.01	0.01	0.28
5	#E / #D	0.38	0.57	0.49	0.98
6	#F / #D	0.02	0.02	0.02	0.30
7	#G / #D	0.01	0.02	0.02	0.22
8	#F / #E	0.05	0.04	0.05	0.31
9	#G / #E	0.04	0.03	0.03	0.23
10	#G / #F	0.69	0.70	0.69	0.73

It is clear that the band ratios labelled as #2 and #5, and highlighted in **Table 3**, are the most suitable for a robust discrimination between the four oil samples. These correspond to the ratios between the fluorescence intensity in the 466 nm - 535 nm spectral range and the intensities in the 410 nm - 430 nm and 430 nm - 465 nm spectral ranges, respectively.

4.3 Slick thickness effects

In order to investigate the behaviour of fluorescence energy conversion efficiency as a function of the slick thickness, four marine diesel slicks samples of different thickness were prepared. The slicks were 70-µm, 100-µm, 140-µm and 210-µm thick. If we consider the spectrally integrated values in the #B spectral band, the energy conversion efficiency E_f shows a quite linear dependency as a function of thickness (r^2 = 0.99, p-value = 0.00039) so that the slick can be considered as optically-thin in the considered thickness range (**Fig. 3**).

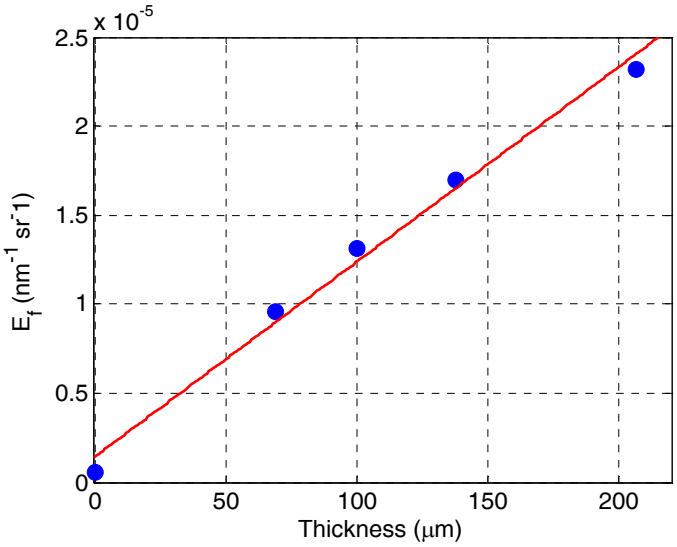

Fig. 3. Fluorescence conversion efficiency - calculated in the #B band - as a function of the slick thickness. The value for the fluorescence spectrum obtained on the synthetic seawater sample (without oil slick) is also reported in the graph for a thickness equal to zero.

This is also consistent with the results obtained for the spectral distribution of conversion efficiency as a function of the oil slick thickness. **Fig. 4** shows the fluorescence spectral distributions of the marine diesel slicks for different thicknesses. In order to distinguish better possible differences in the spectral distribution, the spectra are intensity-normalised to their maximum.

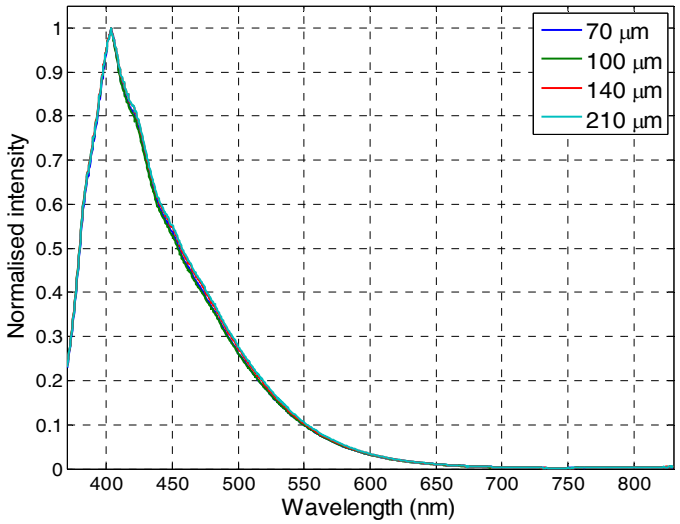

Fig. 4. Fluorescence energy conversion efficiency of the marine diesel for four different oil slick thickness. Spectra are intensity-normalised to the maximum.

From **Fig. 4** it is clear that there are not remarkable differences in the spectral distributions corresponding to different thicknesses; this implies that in this case reabsorption effects can be neglected. The lack of changes suggests also the possibility, at least for this class of oils and up to a slick thickness of some hundreds of micron, of applying discrimination and classification methods based on the fluorescence spectral distribution without performing any correction for the slick thickness.

4.4 Weathering effects

The fluorescence behaviour of the oil slicks was also studied along time to determine possible slick weathering effects on the spectral shape. **Fig. 5** shows the temporal behaviour of the spectral shape for the four samples.

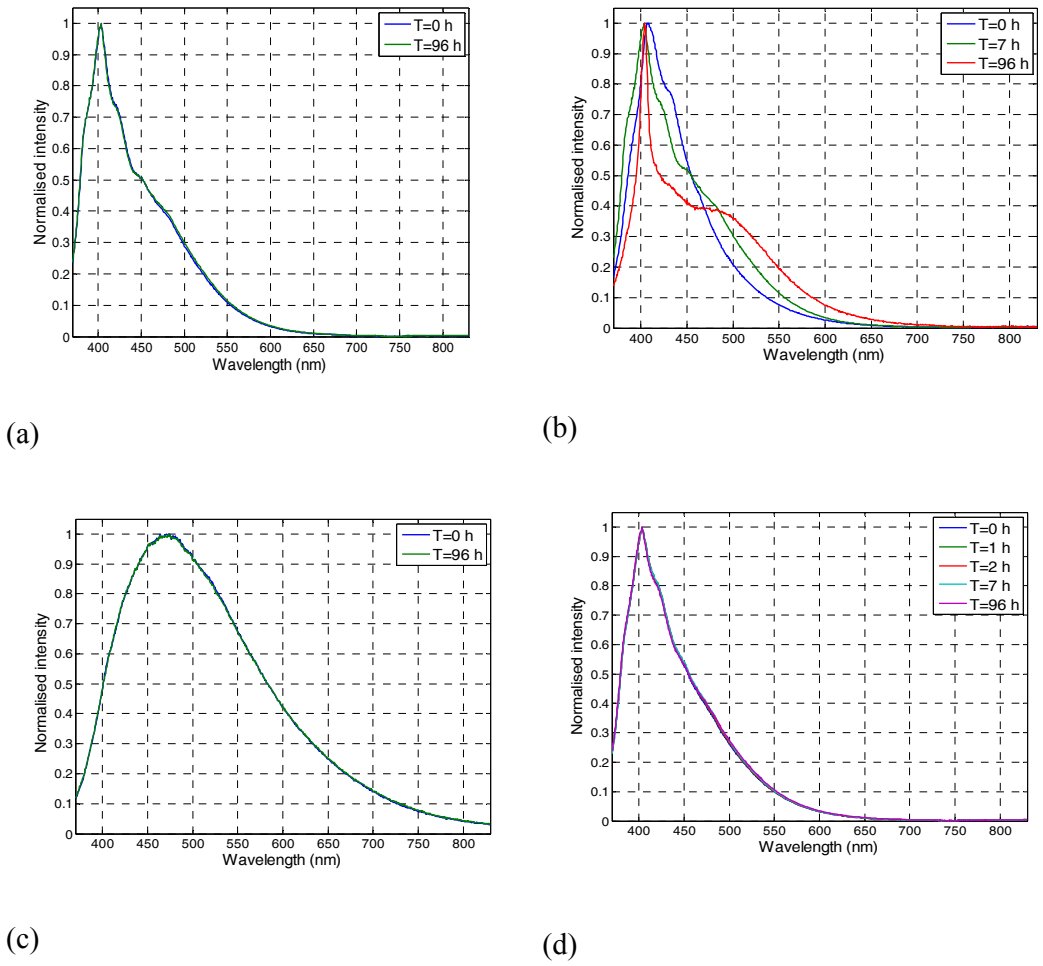

Fig. 5. Weathering of oil slicks: a) automotive diesel; b) automotive gasoline; c) crude oil; and d) marine diesel.

The spectra are normalised to the maximum. Their spectral behaviour was monitored for a temporal interval of 96 hours, focussing particularly on marine diesel and automotive gasoline behaviours. The spectral shapes of diesel and crude oil were essentially unchanged, while the spectral shape of automotive gasoline varied considerably in the considered time interval. The variation in the spectral shape is also accompanied by a strong variation in the fluorescence intensity of the spectrum, as it can be noticed by comparing the fluorescence intensity with the Raman signal at 404 nm. The marine diesel instead showed very small differences after 96-hour weathering

in the laboratory. These small differences are shown in Fig. 6a where the spectral behaviour in the 490 nm - 520 nm range is reported in detail. These variations can be exploited to identify a suitable spectral bands ratio to represent the variation of the oil slick along time.

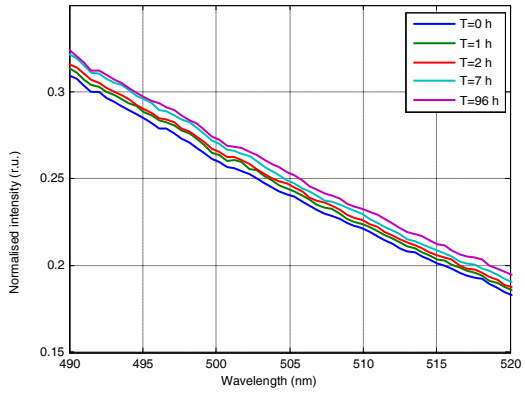

(a)

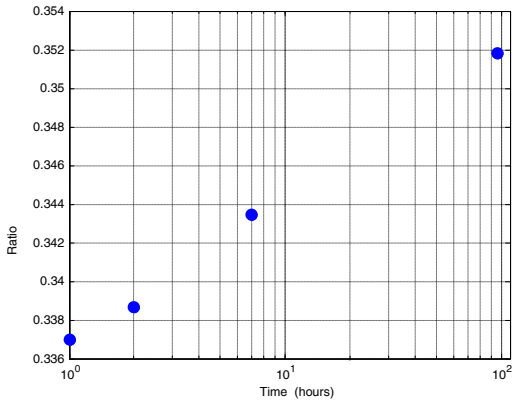

(b)

Fig. 6. Weathering of marine diesel sample in the 490 nm – 520 nm spectral range: (a) Fluorescence spectral behaviour versus time. (b) Ratio between the #D (466 nm - 535 nm) and #C (410 nm - 430 nm) bands versus time. Time is reported in logarithmic scale.

Fig. 6b shows the ratio between the #D (466 nm - 535 nm) and #C (410 nm - 430 nm) bands in semilogarithmic scale. Also in this case the variations of the spectral shape can be mainly attributed to the lighter fractions evaporation since there is a decrease of the contribution of the #C band (410 nm - 430 nm) with respect to the #D band (466 nm - 535 nm). This trend is consistent with the typical evolution of oil spill weathering due to evaporation. It should be noted, however, that the weathering conditions in the laboratory are considerably different from actual weathering conditions in the sea. A major cause of weathering consists in all those effects due to the mechanical action of the waves on the oil slick, such as: the formation of emulsions, solubilisation (and the dispersion within the water column), sedimentation on the floor, aggregation phenomena due to the presence of suspended sand grains. In addition, biodegradation also plays a role in the slick weathering since it reduces the effects of photoreaction on the oil. The lack of these phenomena in the experiment conducted in the laboratory made it dominant the effect due to the evaporation of the lighter fractions, which are more abundantly present in the automotive gasoline sample than in the other samples.

4.5 Radiometric calculations

The energy E_F (λ, R) at a given wavelength λ impinging on the sensor placed at a distance R from the sea surface can be described by the equation:

$$E_F(\lambda,R) = E_L \cdot K_0(\lambda) \cdot T_L(R) \cdot T_F(R) \cdot \xi(R) \cdot \frac{A_0}{R^2} \cdot \eta_F(\lambda,\lambda_L) \ , \qquad (1)$$

Where:

E_L is the laser energy;

K_0 (λ) is a filter function that takes into account the spectral bandwidth, the optics efficiency and the detector efficiency;

T_L (R) and T_F (R) are the air transmittance at a distance R and at wavelength λ_L and wavelength λ, respectively;

ξ (R) is the form factor of the LIDAR;

A_0 is the LIDAR collecting optics area;

η_F (λ, λ_L) is the oil fluorescence conversion efficiency per wavelength λ per solid angle with excitation at wavelength λ_L.

The solar background E_B (λ, R) at a given wavelength λ impinging on the sensor placed at a distance R from the sea surface was evaluated according to the following equation:

$$E_B(\lambda, R) = I_S(\lambda) \cdot w_g \cdot A_S \cdot K_0(\lambda) \cdot T_F(R) \cdot A_{fov} \cdot \frac{A_0}{\pi R^2} \ , \qquad (2)$$

Where:

I_S (λ) is the solar irradiance at wavelength λ on the sea surface;

w_g is the detector gating time;

A_s is the albedo;

A_{fov} is the FOV area of the LIDAR system.

In order to carry out radiometric calculations, the main technical characteristics of the LIDAR system were defined. **Table 4** reports the main technical data used for the radiometric calculations.

Table 4. Operational conditions and LIDAR main technical specifications.

Laser Source	Excitation wavelentgh: 355 nm Output energy: 50 μJ @ 355 nm Pulse repetition rate: 10 kHz
System parameters	Spectral sampling: 3 nm System filter function: 0.15 (optics and detector efficiency,spectral bandwidth) IFOV: 3 mrad
Acquisition parameters	Gate width: 50 μm Acquisition rate: 20 Hz
Operational conditions	Spot at sea: 30-cm diameter Platform speed: 30 km/h Altitude: 100 - 1000 m

A tripled frequency Nd:YAG laser emitting at 355 nm was chosen as an excitation source. This is a solid state laser that offers several advantages in terms of robustness, reliability and maintenance. Several very compact models are already available on the market featuring output energy in the range of 30 μJ - 60 μJ and a pulse repetition rate of several kHz. In addition, an excitation source in the spectral range between 300 nm and 355 nm provides substantial advantage in terms of eye safety with respect to a source in the visible. For example, the MPE (Maximum Permissible Exposure) for a laser in the UV at 355 nm is more than two orders of magnitude higher than that of a laser in the visible at 532 nm.

The efficiency of the LIDAR optics was set to 70%, detector efficiency was 30% and fibre optics coupling factor was set to 0.25. The LIDAR geometric factor was equal to

0.7. Considered the relatively low altitude of the platform, the air transmittance was considered equal to 1 at both the fluorescence and excitation wavelengths all through the path.

As far as the operational conditions are concerned, a 30-cm diameter spot at the target (sea surface) for a platform altitude of 100 m was considered. This implied an IFOV of 3 mrad for the system, to be matched by using a proper conditioning optics on the transmitting section, depending on the divergence of laser source used. The IFOV determined also the collection optics main characteristics, taking also into account the numeric aperture of the selected dispersion and detection system. A collecting optics of about 80-mm diameter with an *f/4* numeric aperture were applied.

For each measurement, the fluorescence signal was supposed to be accumulated over several laser pulses. This, in fact, allows to minimise the contribution of the background radiation, of the readout noise and to improve the signal to noise ratio and the duty cycle. The number of laser pulses (accumulations) can be calculated so as to obtain an along-track dimension of the measured area equal to twice the across track dimension that, on turn, is determined by the IFOV of the LIDAR system. This means that the laser spot at the target has moved in the along track direction of a distance equal to the laser spot diameter. If we assume a repetition rate for the laser source of 10 kHz and a platform speed of 30 km/h, the fluorescence signal will be accumulated over 360 pulses and the measured area at the sea surface will have an across- and along-track dimensions of 30 cm and 60 cm, respectively, from an altitude of 100 m. The number of laser pulses to accumulate for each measurement can be varied automatically and dynamically depending on the characteristics of the target in order to obtain an acceptable signal to noise ratio.

The oil slick was supposed to be of a 20-mm thickness and uniformly distributed over the sea surface. The maximum oil conversion efficiency values - per wavelength unit (nm^{-1}) and per solid angle unit (sr^{-1}) – for an oil thickness of 20 μm are reported in **Table 5**. These values were retrieved from the fluorescence conversion efficiency spectra measured in the laboratory on the four oil samples (Fig. 1) by assuming that conversion efficiency and oil thickness are linearly dependent in the considered thickness range.

Table 5. Maximum fluorescence conversion efficiency of the samples (slick thickness: 20 μm; excitation wavelength: 355 nm).

	Fluorescence conversion efficiency (nm^{-1} sr^{-1})
Automotive diesel	$5.1\ 10^{-6}$
Automotive gasoline	$1.2\ 10^{-6}$
Crude oil	$2.4\ 10^{-6}$
Marine diesel	$2.7\ 10^{-6}$

The radiometric calculations were carried out for different operational altitudes of the platform, from 100 m to 1000 m, varying the number *N* of accumulations over laser pulses according to the altitude. The number of accumulations was determined in order to obtain the along-track dimension of the measured area equal to twice its across-track dimension.

The signal to noise ratio (SNR) was evaluated according to the following equation:

$$SNR = \sqrt{N} \cdot \frac{N_F}{\sqrt{N_F + 2N_B}}, \quad (3)$$

Where N is the number of accumulations and N_F and N_B are the number of photons collected as fluorescence signal and as background signal, respectively. Taking into account equations (1) and (2), the latter are given by:

$$N_F(\lambda, R) = \frac{E_F(\lambda, R)}{\frac{hc}{\lambda}}, \qquad N_B(\lambda, R) = \frac{E_B(\lambda, R)}{\frac{hc}{\lambda}}. \tag{4}$$

Table 6 reports the SNR calculated for the #D band (430 nm – 465 nm) for different altitudes of the platform (100 m - 1000 m).

Table 6. Signal-to-noise ratio (SNR) as a function of the altitude. The UAV speed is 30 km/h.

Altitude (m)	Measured spot diameter (m)	Nr. of integrated laser pulses	SNR			
			Automotive Gasoline	Automotive Diesel	Marine Diesel	Crude Oil
100	0.30	360	16.5	56.2	33.1	30.1
125	0.38	450	12.2	43.8	25.0	22.6
150	0.45	540	9.4	35.1	19.6	17.7
200	0.60	720	6.2	24.2	13.2	11.9
250	0.75	900	4.5	17.8	9.6	8.6
300	0.90	1080	3.4	13.8	7.4	6.6
350	1.05	1260	2.7	11.1	5.9	5.3
400	1.20	1440	2.2	9.1	4.8	4.3
450	1.35	1620	1.9	7.7	4.1	3.6
500	1.50	1800	1.6	6.6	3.5	3.1
600	1.80	2160	1.2	5.0	2.6	2.4
700	2.10	2520	1.0	4.0	2.1	1.9
1000	3.00	3600	0.6	2.4	1.2	1.1

The signal to noise ratio is good for the all types of oils up to an altitude of some hundreds of meters, except for the automotive gasoline that shows a signal to noise ratio < 10 even at an operational altitude of 150 m.

The radiometric calculations were also used to assess the performance of the discrimination method based on the ratios between the selected bands reported in **Table 3**. The results are shown in **Fig. 7**, where the ratios between the #E and #C spectral bands (**Fig. 7**a) and between the #E / #D spectral bands (**Fig. 7**b) are reported together with the corresponding uncertainties (σ). The platform altitude considered for this evaluation was 200 m.

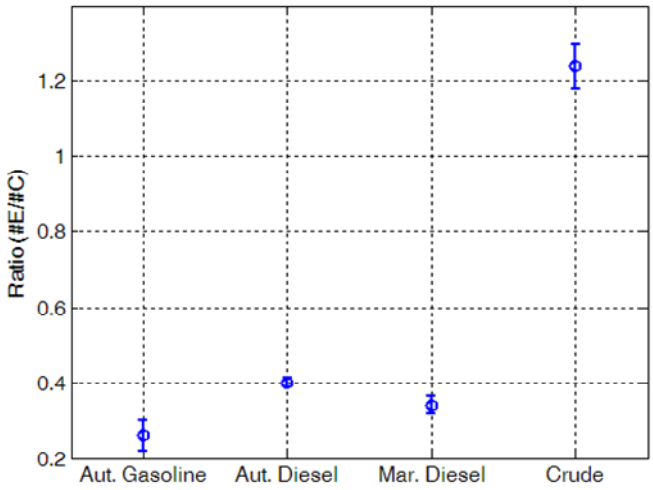

(a)

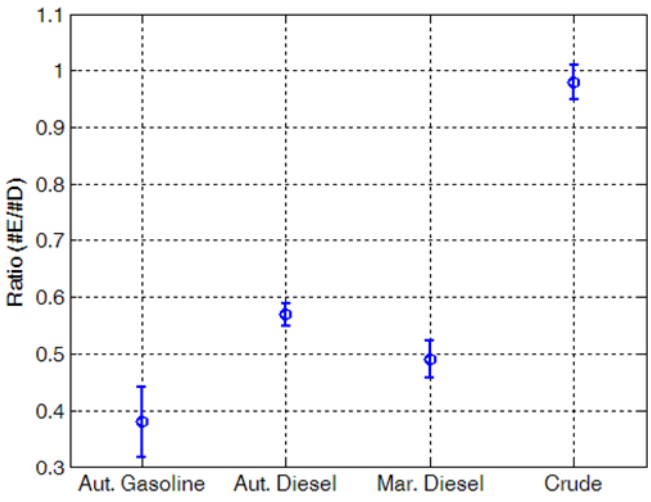

(b)

Fig. 7. Ratios of the selected spectral bands calculated for the four oil samples: (a) #E / #C ratio. (b) #E / #D ratio. The platform altitude is 200 m and the oil spill thickness is 20 μm.

Both the ratios perform quite well to discriminate the samples, although the automotive diesel and the marine diesel still have quite similar values.

CONCLUSIONS

The feasibility to develop a UAV-based fluorescence LIDAR system for oil slicks detection and discrimination in the sea was investigated by means of LIDAR measurements on oil samples in the laboratory and radiometric calculations.

The LIDAR measurements, conducted on samples of gasoline, automotive diesel, crude oil and marine diesel, were used to determine their oil fluorescence conversion efficiencies and to propose a simplified discrimination method relying on the acquisition of a limited number of spectral bands (7 bands distributed in the 350 nm - 750 nm range) in order to reduce the payload requirements. The maximum fluorescence

conversion efficiency per nanometer and per solid angle, retrieved for a slick thickness of 20 μm and with excitation at 355 nm, were 5.1 10^{-6} for the automotive diesel, 1.2 10^{-6} for the automotive gasoline, 2.4 10^{-6} for the crude oil and 2.7 10^{-6} for the marine diesel.

The effects of slick thickness from 70 μm to 210 μm and weathering along 96 hours were studied in relation to the proposed discrimination method. Results showed that the slick thickness does not significantly affect the results obtained with the proposed discrimination method in the investigated thickness range. Weathering was found to be a negligible issue for most samples, except for the automotive gasoline sample, as expected. This result is consistent with the high content in lighter fractions for this sample. It should be anyway underlined that the simulation of weathering in the laboratory does not take into account several phenomena that occur in the field, such as the mechanical action of the waves.

Finally, the main technical specifications of the LIDAR payload were outlined and radiometric calculations performed to assess the feasibility of oil detection by using a UAV-based LIDAR and of oil discrimination by using the proposed method. The signal to noise ratio was good at an operational altitude of 100 m and still acceptable (>10) up to an altitude of 200 m for all oils, except for the automotive gasoline that showed a poor signal to noise ratio even at an operational altitude of 150 m. The proposed method showed a good performance that is still acceptable up to an altitude of 200 m to discriminate the considered oil samples from each other. The next step will be to extend the set of oil samples to test.

In principle, the technique and the method illustrated in this paper can be also applied to other operative scenarios that have not been investigated here, such as spills floating below the sea surface or oil-water emulsions. These applications, however, could require the use of more performing components, such as a higher output energy for the

excitation source and an increased sensitivity of the detection system due to the need of penetrating the water column on both the excitation and collection paths. Considering the actual fast rate of technological development in miniaturised optoelectronic components, such items could be soon available on the market in the near future.

ACKNOWLEDGEMENTS

This study was carried out in the frame of the ALTRO (Active Laser TransReceiver Optical) project funded by the Regione Toscana under the *"Bando Unico R&D 2008" – Linea A* research and development programme.

REFERENCES

[1]. Coleman J, et al. Oil in the sea III: Inputs, Fates, and Effects. The National Academy of Sciences, The National Academies Press, Washington, D.C. 2003.

[2]. Alpem B, et al. Detection and evaluation of hydrocarbons insource rocks by fluorescence microscopy. Org Geochem 1993;20(6):789-795.

[3]. Palombi L, et al. Fluorescence LIDAR remote sensing of oils: merging spectral and time-decay measurements. SPIE Remote Sensing 2013;88870F-88870F-8.

[4]. Brown CE Fingas MF. Review of the development of laser fluorosensor for oil spill application. Marine Pollution Bulletin 2003;47:477-484.

[5]. Balick L, et al. Fluorescence Emission Spectral Measurements for the Detection of Oil on Shore. Proceedings of the Fourth Thematic Conference on Remote Sensing for Marine and Coastal Environments, Environmental Research Institute of Michigan, Ann Arbor, Michigan. 1997;I:13-20.

[6]. Camagni P, et al. Diagnostics of Oil Pollution by Laser-Induced Fluorescence. IEEE Transactions on Geoscience and Remote Sensing 1988;GE-26(1):22-26.

[7]. Chubarov VV, et al. New remote method for measurement of oil slick thickness on water surface. In: Third Thematic Conference on Remote Sensing for Marine and Coastal Environments 1995;1:433-440.

[8]. Delaune PL, et al. Enhanced wellsite technique for oil detection and characterization. SPE-56802, in SPE annual technical conference and exhibition proceedings, Formation evaluation and reservoir geology 1999;801-816.

[9]. Fantasia JF, Ingrao HC. The Development of an Experimental Airborne Laser Remote Sensing System for the Detection and Classification of Oil Spill. In: Proceedings of the 9th International Conference on Remote Sensing of Environment, Ann Arbor, Michigan, 1974;3:1711-1745.

[10]. Goodman R, Overview and future trends in oil spill remote sensing. Spill Science & Technology Bulletin 1994;1:11–21.

[11]. Jha MN, et al. Advances in remote sensing for oil spill disaster management:state-of-the-art sensors technology for oil spill surveillance. Sensors 2008;8:236–255.

[12]. Guilhaumou N, et al. Characterization of hydrocarbon fluid inclusions by infra-red and fluorescence microspectrometry. Mineral Mag 1990;54:311-324.

[13]. Hagemann, HW, Hollerbach, A. The fluorescence behavior of crude oils with respect to their thermal maturation and degradation. Org Geochem 1986;10:473-480.

[14]. Hegazi E, et al. Remote Fingerprinting of Crude Oil Using Time-Resolved Fluorescence Spectra. The Arabian Journal for Science and Engineering 2005;30(1B):3-12.

[15]. Hoge FE, Swift RN. Oil film thickness measurement using airborne laser-induced water Raman backscatter. Appl Opt 1980;19:3269-3281.

[16]. Babichenko S, et al. Laser remote sensing of coastal and terrestrial pollution by FLS-lidar. EARSeL eProceedings 2004;3(1):1-8.

[17]. Lennon M, et al. Operational quantitave mapping of oil pollutions at sea by joint use of a hyperspectral imager and a fluorescence lidar system on-board a fixed-wing aircraft. In: IEEE OCEANS 2005, Brest, France, 2005.

[18]. Li J, et al. Matching fluorescence spectra of oil spills with spectra from suspect sources. Anal Chim Acta 2004;514(1):51-56.

[19]. Masahiko S, et al. Development of a helicopter-based fluorescence imaging lidar for oil spill monitoring. Journal of the Visualization Society of Japan 2005;25 (1): 421-424.

[20]. Measures RM, et al. Laser induced fluorescent decay spectra - a new form of environmental signature. Opt Eng 1974;13(6):494-501.

[21]. Palombi L, et al. A fluorescence LIDAR sensor for hyper-spectral time-resolved remote sensing and mapping. Optics Express 2013;21(12):14736-14746.

[22]. Patsayeva S. Fluorescent remote diagnostics of oil pollutions: oil in films and oil dispersed in the water body. EARSeL Advances in Remote Sensing 1995;3(3):170-178.

[23]. Patsayeva S, et al. Laser Spectroscopy of mineral oils on the water surface. EARSel eProceedings 2000;1(1):106-114.

[24]. Pharr DY, et al. Fingerprinting Petroleum Contamination Using Synchronous Scanning Fluorescence Spectroscopy. Ground Water 1993;30(4):484-489.

[25]. Piskozub J, et al. A lidar system for remote measurements of oil film thickness on sea surface. In: Proceedings of Fourth International Conference on Remote Sensing for Marine and Coastal Environments. Technology and Applications, ERIM, 1997;I-386.

[26]. Pradier B, et al. Chemical basis of fluorescence alteration of crude oils and kerogens .1. Microfluorimetry of an oil and its isolated fractions - relationships with chemical-structure. Org Geochem 1990;16(1-3):451-460.

[27]. Raimondi V, et al. Design and development of a new high speed performance fluorescence imaging lidar for the control of indoor and outdoor cultural heritage. In: Castillejo, M., Moreno, P., Oujja, M., Radvan, R., Ruiz, J., (Eds.), Lasers in the Conservation of Artworks, Proceedings of the International Conference Lacona VII, CRC press, 2008;163-168.

[28]. Reuter R, et al. A laser fluorosensor for maritime surveillance: Experimental results. EARSeL Advances in Remote Sensing 1995;3(3):152-169.

[29]. Ryder AG. Quantitative analysis of crude oils by fluorescence lifetime and steady state measurements using 380 nm excitation. Appl Spectrosc 2002;56(1):107-116.

[30]. Stasiuk LD, Snowdon LR. Fluorescence micro-spectrometry of synthetic and natural hydrocarbon fluid inclusions: crude oil chemistry, density and application to petroleum migration. Appl Geochem 1997;12(3):229-233.